Ocean Systems Engineering, *Vol. 8, No. 4 (2018) 361-380*
DOI: https:// doi.org/10.12989/ose.2018.8.4.361

A study on performance assessment of WEC rotor in the Jeju western waters

Sunny Kumar Poguluri[a] and Yoon Hyeok Bae[*]

Department of Ocean System Engineering, Jeju National University,
102 Jejudaehak-ro, Jeju-si, Jeju Special Self-Governing Province, 63243, Republic of Korea

(Received July 12, 2018, Revised September 19, 2018, Accepted September 21, 2018)

Abstract. The dynamic performance of the wave energy converter (WEC) rotor with different geometric parameters such as depth of submergence and beak angle has been assessed by considering the linear potential flow theory using WAMIT solver and along with the computational fluid dynamics (CFD). The effect of viscous damping is incorporated by conducting numerical free decay test using CFD. The hydrodynamic coefficients obtained from the WAMIT, viscous damping from the CFD and estimated PTO damping are used to solve the equation of motion to obtain the final pitch response, mean optimal power and capture width. The viscous damping is almost 0.9 to 4.6 times when compared to the actual damping. It is observed that by neglecting the viscous damping the pitch response and power are overestimated when compared to the without viscous damping. The performance of the pitch WEC rotor in the Jeju western coast at the Chagwido is analyzed using Joint North Sea Wave Project (JONSWAP) spectrum and square-root of average extracted power is obtained. The performance of WEC rotor with depth of submergence 2.8 m and beak angle 60° found to be good compared to the other rotors.

Keywords: wave energy converter (WEC) rotor; viscous damping; CFD simulation; square-root of average extracted power

1. Introduction

In the history, it has been recognized that the enormous of energy potential available in ocean waves and these waves are generated due to the interaction between wind and water surface. The total energy of a wave depends mainly on two factors wave height and period. A good wave energy converter (WEC) should able to absorb the incident wave by generating counter waves. The ability of the wave energy absorption/converter depends on its hydrodynamic design and motion of the hull relative to the waves. Much knowledge has been gained through the extensive work performed on the WEC and their developments are reviewed in past by many, see Bhattacharyya and McCormick (2003), Cruz (2007), Cho *et al.* (2012) and Cho and Kim (2013). One of the most representative ways is the classification of WEC proposed by Antonio (2010) which groups the devices into three main categories. 1. Oscillating water columns 2. Overtopping devices and 3. Wave-activated bodies. A comprehensive report on wave energy technologies and conceptual

∗Corresponding author, Professor, E-mail: yh.bae@jejunu.ac.kr
[a] Ph.D., E-mail: sunnykumar@jejunu.ac.kr

 ISSN: 2093-6702 (Print), 2093-677X (Online)

design based on theoretical and numerical techniques has been reviewed, discussed and presented in Falnes (2002, 2007), Cruz (2007), Antonio (2010) and Folley (2016). Under wave-activated bodies, Salter in 1974 spurred from his research work on non-symmetrical duck-shaped floating body (called as Salter's duck see Fig. 1) as one of the most efficient WEC which can tap 90% of wave energy in two-dimensional sinusoidal waves. The essential geometric features of the Salter's duck were based on the efficient hydrodynamic shape. Later, Evan (1976) proposed a theoretical based approach on a two dimensional fully submerged cylinder to generate waves only in one direction by tuning the amplitudes and phases of the heave and surge motions and reversing the sign of time coordinate showed an 100% absorption of the incident wave. In the same year, Mei came out with a design based on tethered-float breakwater to obtain the maximum extraction of power out from the waves by a two dimensional floating body. Mei concluded that the maximum extraction is possible when the WEC and the fluid oscillates at resonance in single degree of freedom and is greater for non-symmetrical bodies. Based on the Salter's duck, studies were extensively carried out, reported and documented by Edinburgh wave power group (Salter *et al*. 1975, Jeffrey *et al.* 1976). From now on, the duck will be referred as WEC rotor in the present study. The cross section of the WEC rotor comprises of stern (circular in shape), paunch (exponential form) and beak (see Fig. 1). The geometry shape of the nodding WEC rotor at paunch part has arrived based on the fluid particle displacement. The outcome from the Edinburgh wave power group includes enormous amount of experimental wave tank data on a model scale were performed to improve the design and performance of the WEC rotor. Following them, Count (1978) showed excellent performance of the WEC rotor comparable with the experimental data for the shape of the rotor by solving the hydrodynamic forces using two dimensional source distribution methods. Mynett *et al*. (1979) studied the performance and hydrodynamic effect of the WEC rotor due to geometric changes based on hybrid numerical model using finite element method near the body and analytical method in the remaining domain. They concluded that less non-symmetric profiles have minor influence on the optimal performance and it decreases with increasing the degree of freedom. Skyner (1987) reported model scale study on solo duck whose hydrodynamic quantities measured through a suspended rig from the above water surface. Rig is used to measure the force and velocity in pitch, heave and surge motions. Based on radiation impedance matrix the interaction of the solo duck motion and the fluid are given. Where the real part of the radiation impedance matrix comes from the added damping and imaginary part is due to the solo duck inertia and water added mass. Skyner obtained the maximum performance in both regular and irregular waves. Pizer (1994) developed a linear three dimensional numerical method based on the pulsating Green's function used on the wetted surface of the solo duck. The wetted surface of the geometry is defined by an automated algorithm to generate mesh using triangular or rectangular facets. For different geometry configurations and wave conditions the solo duck efficiency was calculated. Many authors expanded the scope of application of WEC rotor to realistic environmental conditions (see Pecher *et al.* 2015) to full scale. Weptos WEC with extensive research and development is based on Salter's duck design are able to come out with commercial WEC's at different locations like Danish North Sea Pt1 & Pt3, EMEC and Yeu Island. The patented A-shaped structure which has the capability to adjust the angle between the two legs, wide angles are maintained during small wave conditions and closed during storm period which enables stable power productions in various environmental conditions. A rigorous lab tests, focusing on hydrodynamic performance of the WEC rotor helped its structural and mooring line integrity with the main frame structure for various wave and extreme conditions to come out with the full scale WEC.

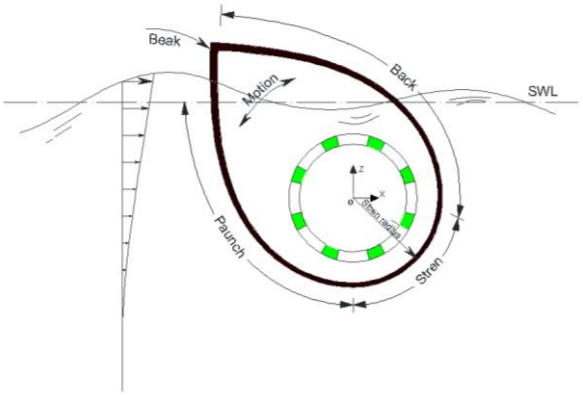

Fig. 1 Nomenclature of the nodding WEC rotor

With this knowledge, the present work focuses on design performance of the WEC rotor, to suite the Jeju western waters for a water depth of 80m. Detailed parametric studies are conducted numerically on the WEC rotor based on the depth of submergence (draft) and beak angle. The dynamics of the WEC rotor will be systematically assessed by considering hydrodynamic coefficients such as added mass, radiation damping and wave exciting force using WAMIT. The equation of motion of WEC rotor is solved in the frequency domain by incorporating the viscous damping as an external quantity obtained from free decay test conducted in computational fluid dynamics (CFD) using STAR-CCM+. Section 2 gives the details of the WEC rotor. Section 3 presents the mathematical aspects of the hydrodynamic relevant and the equation of motion of the WEC rotor. The calculation of mean optimal power and capture width are also described. Section 4 deals with the validation and numerical analysis which includes WAMIT and CFD. Finally in Sections 5 and 6 results, discussion and conclusions are presented.

2. Geometry modeling

The fundamental geometry of WEC rotor is adopted from Jeffrey *et al.* (1976). The geometric parameters are kept constant with the model except the width other parameters are scaled to 20 times compare to the model. Consider normal incidence and x and z denote the mean position of the center of the rotation (point O) and ξ the rotational displacement (Fig. 2).

The WEC rotor is 5 m long in y-direction whose isometric view is shown in Fig. 3. The rotor is situated in a water depth (h) of 80 m. The paunch of the duck obtained by an exponential profile ($R=re^{\frac{2\pi}{\lambda}b}$) rotates about point O where 'r' is the stern radius, 'λ' taken as 40m and 'b' is ordinate from the base of rotor.

The paunch of the WEC rotor is shaped such that the dynamic pressure caused by the wave-induced water particle motions efficiently forces the duck to rotate about an axis through point O. In addition to the dynamic pressure, the changing hydrostatic pressure contributes to the rotation by causing the buoyant forebody near the beak to rise and fall.

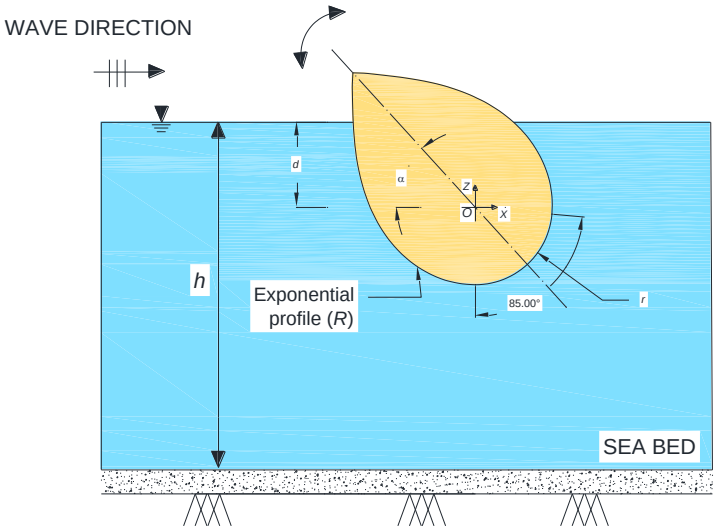

Fig. 2 Schematic representation of the WEC rotor geometry

Table 1 Dimensions, hydrostatic and inertia properties for various WEC rotors

Description	Prototype					
	D0.7a36	D0.7a48	D0.7a60	D0.8a36	D0.8a48	D1.05a60
Stern diameter, $2r$ (m)	4.0					
Depth of submergence, d (m)	2.8	2.8	2.8	3.2	3.2	4.2
Beak angle, α (deg)	36	48	60	36	48	60
Width, W (m)	5.0					
Water depth, h (m)	80.0					
Rotor mass (kg)	15219.87					
Total mass (kg)	22751.83	19272.09	17298.03	27740.25	23631.83	38712.05
Ballast mass (kg)	7531.96	4052.22	2078.16	12520.38	8411.96	23492.18
Pitch moment of inertia about center of rotation (kg.m^2)	134517.83	119857.18	110580.81	170602.60	139589.50	209066.88
Hydrostatic coefficient, $K_{55}/\rho g$	41.32	39.46	12.74	57.26	31.46	41.11
Horizontal center of gravity (m)	-1.1274	-0.8771	-0.6174	-1.2375	-0.9677	-0.5692
Vertical center of gravity (m)	0.4101	0.5842	0.7661	0.2871	0.5991	0.8396
Natural frequency, ω_N (rad/s)	1.53	1.56	1.03	1.57	1.34	1.17

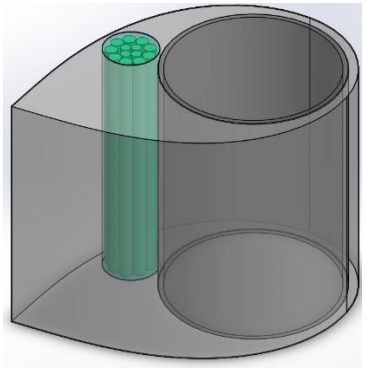

Fig. 3 Geometry modeling in Solidworks

Since both of these pressure-induced motions are in phase, the nodding WEC rotor converts both the kinetic and potential energies of the wave into rotational mechanical energy. In the present study, configurations of WEC rotor for analysis were considered by changing the depth of submergence and beak angle, whose principle particulars, inertia and hydrostatic properties are listed in Table 1. Few cases has been omitted from the analysis due to spurious oscillations observed in the pitch response and this aspect needs further investigation and has been left out of the present scope. The mass property along with the moment of inertial about *y* is calculated using solid modeler (Solidworks®) software. The hydrostatic restoring pitch coefficient (K_{55}) was obtained from the WAMIT software (see Table 1).

3. Mathematical model

In time domain, assuming the pitch motion of the WEC rotor is uncoupled from motions at other degrees of freedom, the governing equation of motion of rotor is given as (Falnes 2002, Mei *et al.* 2005)

$$M_{55}\ddot{\zeta}_5(t) = F_5^P(t) + F_5^R(t) + F_5^{vis}(t), \tag{1}$$

where the subscript '5'corresponds to pitch motion of WEC rotor and 'dot' represent the time derivative. The types of total moment on a WEC rotor include the force due to the external pressure ($F_5^P(t)$), the reaction moments $F_5^R(t)$ which typically includes the loads induced by the power-take-off (PTO), and mooring lines if any connected and viscous moment $F_5^{vis}(t)$. Considering the angular displacement between the WEC rotor and the waves as a harmonic function of time represented by ξ

$$\zeta_5(t) = \mathrm{Re}\left\{\xi_5 e^{-i\omega t}\right\} \tag{2}$$

where ω angular frequency of the exciting wave and corresponding velocity and acceleration are given respectively as

$$\dot{\zeta}_5(t) = \mathrm{Re}\left\{-i\omega\xi_5 e^{-i\omega t}\right\} \quad \text{and} \quad \ddot{\zeta}_5(t) = \mathrm{Re}\left\{\omega^2\xi_5 e^{-i\omega t}\right\} \tag{3}$$

The moment due to the external pressure on the WEC rotor decomposes of hydrodynamic $(F_5^{dynamic}(t))$ and hydrostatic components $(F_5^{static}(t))$. Again $F_5^{dynamic}(t)$ consists of wave excitation moment $(F_5^{ext}(t))$ and the radiation moments $(F_5^{rad}(t))$. The radiation moment is due to the harmonic body motion in otherwise calm water. This has a component proportional to body acceleration and a component proportional to body velocity is given by $(F_5^{rad}(t) = -A_{55}\ddot{\zeta}_5 - B_{55}^{rad}\dot{\zeta}_5)$. $F_5^{static}(t)$ is the resultant of the buoyancy and gravity where the hydrostatic pressure distribution around the wetted surface of the rotor in an undisturbed position can be written as $-K_{55}\zeta_5$. The reaction moments are $F_5^{PTO}(t) = -B_{55}^{PTO}\dot{\zeta}_5$ due to the PTO and the viscous moment by $-B_{55}^{vis}\dot{\zeta}_5$. Substituting these quantities on the right hand side of Eq. (1) and rearranging, the equation of motion for the WEC rotor in pitch mode can be written as (Falnes 2002)

$$\left[K_{55} - (J + A_{55})\omega^2 + i(B_{55}^{rad} + B_{55}^{vis} + B_{55}^{PTO})\omega\right]\xi_5 = aX_5; \tag{4a}$$

$$\left|\frac{\xi_5}{a}\right| = \frac{|X_5|}{\sqrt{\left[(K_{55} - (J + A_{55})\omega^2)^2 + (B_{55}^{rad} + B_{55}^{vis} + B_{55}^{PTO})^2\omega^2\right]}} \tag{4b}$$

where '*a*' wave amplitude, '*J*' mass moment of inertia of the WEC rotor, 'B_5^{rad}, B_5^{vis} and B_{55}^{PTO}' are radiation, viscous and PTO damping. The coefficients, A_{55}, K_{55} and X_5 are the added mass inertia, hydrostatic stiffness moment and wave excitation moment. These coefficients are obtained through WAMIT. The mean power absorption which can be obtained by the mean power consumed by the PTO from an incident wave by means of a WEC rotor is

$$\bar{P} = \frac{1}{2}\omega^2 B_{55}^{PTO} \frac{a^2|X_5|}{\sqrt{\left[(K_{55} - (J + A_{55})\omega^2)^2 + (B_{55}^{rad} + B_{55}^{vis} + B_{55}^{PTO})^2\omega^2\right]}} \tag{5}$$

The optimum control for maximizing converted power $(\bar{P}_{\max}(\omega))$ can be extracted in two major conditions. The first condition states that the optimum PTO damping can be obtained from $\partial\bar{P}/\partial B_{55}^{PTO} = 0$ and is given by

$$\tilde{B}_{55}^{PTO} = \frac{\sqrt{(\omega_N^2 - \omega^2)^2(J + A_{55})^2 + (B_{55}^{rad} + B_{55}^{vis})^2\omega^2)}}{\omega} \tag{6}$$

The second condition states that WEC rotor has to resonate at its natural frequency (i.e., $\omega = \omega_N$) where ω_N is the pitch natural frequency of the WEC rotor. In this condition, the WEC rotor velocity moves in phase with the excitation force. The control strategy that provides these two conditions is typically called as complex-conjugate control. At resonance PTO damping equals

the sum of radiation damping and viscous damping ($B_{55}^{PTO} = B_{55}^{rad} + B_{55}^{vis}$). This means a WEC rotor can absorb the incident wave by generating counter waves. The maximum mean power of a WEC rotor can be extracted by incorporation of these conditions for a single mode as

$$\bar{P}_{\max}(\omega) = \frac{1}{8} a^2 \frac{\left|X_5\right|^2}{B_{55}^{rad} + B_{55}^{vis}} \tag{7}$$

The optimum mean power can be determined using Eq. (6) and the capture width means the ratio of the mean power absorption to the incident power, and therefore both are given by

$$\bar{P}_{opt}(\omega) = \frac{1}{2} \omega^2 \tilde{B}_{55}^{PTO} a^2 \left|\frac{\xi_5}{a}\right|^2 , \tag{8}$$

$$l_{opt}(\omega) = \frac{\bar{P}_{opt}(\omega)}{\frac{1}{2}\rho g a^2 C_g} \tag{9}$$

where C_g is the group celerity of the wave can be expressed as $\frac{C}{2}\left[1+\frac{2kh}{\sinh 2kh}\right]$ and C is celerity $\frac{gT}{2\pi}\tanh kh$. It may be noted that, the PTO stiffness is assumed to be zero while extracting the power (see Eqs. (7) and (8)).

The WEC is planned to operate in the Chagwido, western coast of the Jeju waters at a water depth of 80 m located at an latitude of 33, 21, 05 and longitude 126, 06, 18. Based on the measured data, Joint North Sea Wave Project (JONSWAP) wave spectrum is chosen for the analysis. The pitch response spectrum of a motion can be obtained by using the transfer function of the pitch motion and the wave spectrum by

$$S_{\xi_5}(\omega) = \left|\frac{\xi_5(\omega)}{a}\right|^2 \cdot S_\zeta(\omega) \tag{10}$$

where the $S_\zeta(\omega)$ is given by the JONSWAP spectrum as given below

$$S_\zeta(\omega) = \beta \frac{H_{1/3}^2 \omega_P^4}{\omega^5} \exp\left[-1.25\left(\frac{\omega}{\omega_P}\right)^{-4}\right] \gamma^{\exp\left[-\frac{(\omega-\omega_P)^2}{2\sigma^2\omega_P^2}\right]},$$

$$\text{with } \beta = \frac{0.0624}{0.23 + 0.0336\gamma - 0.185(1.9+\gamma)^{-1}}(1.094 - 0.01915\ln\gamma), \tag{11}$$

where γ is the peakedness factor, ω_P circular frequency at spectral peak, $H_{1/3}$ is the significate wave height and σ is the step function. Finally, the square-root of power spectrum can be estimated as

the product of mean optimal power and the wave spectrum to the wave amplitude square and is given as (see Kim *et al.* 2014)

$$S_{\sqrt{\bar{P}}}(\omega) = \frac{\bar{P}_{opt}(\omega)}{a^2} S_{\zeta}(\omega) \tag{12}$$

The square-root of average extracted power can be written as (Kim *et al*. 2014)

$$\bar{P}_{irr} = \int_0^{\infty} S_{\sqrt{\bar{P}}}(\omega)\, d\omega \tag{13}$$

It must be noted that the final square-root of power spectral response is obtained based on variable optimal PTO damping. The present paper results are based on the frequency domain analysis so the variable optimal PTO damping usage must be alright. It is more appropriate to use the single PTO damping in the time simulations rather than in the frequency domain analysis. To obtain the PTO damping for the WEC rotor, rigorous lab experimental data is needed. Pecher *et al.* (2012) conducted on WEC rotors on a floating platform to obtain the constant and linear PTO damping.

4. Numerical analysis

The wave forces experienced by WEC rotor falls in two dominate regime of analysis by noting the WEC rotor geometry, wave length and wave height in terms of $\pi D/\lambda$ and H/D. For rotors with a characteristic diameter greater than the 1/6 of a wave length corresponds to the diffraction wave force regime else it augments predominantly with the viscous wave forces see Fig. 4. The WEC rotors considered for analysis in the range of frequencies were depicted in Fig. 4. One can notice that the chosen rotors are scattered over the different regimes which are marked in Fig. 4. So, in the present paper, the solution has been obtained by estimating WEC rotor by both diffraction potential flow theory and viscous forces based on Reynolds-averaged Navier-Stokes (RANS) solver. The equation of pitch motion is solved in frequency domain analysis and the viscous damping shall be incorporated as an external damping.

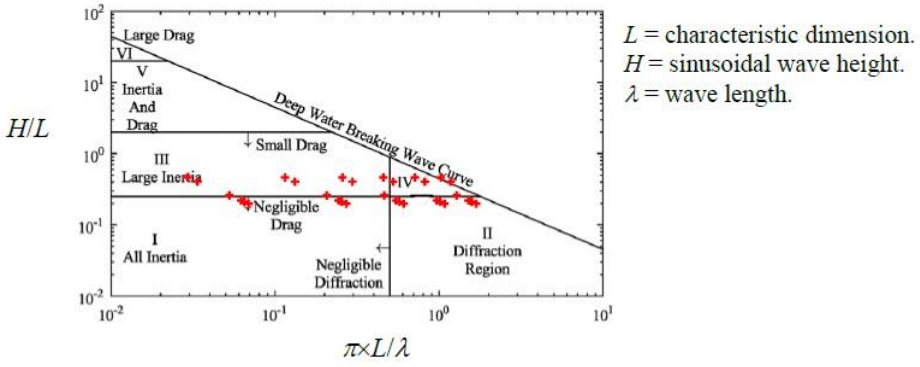

Fig. 4 Different wave force regimes exposed to the WEC rotor (Chakrabarti 2005)

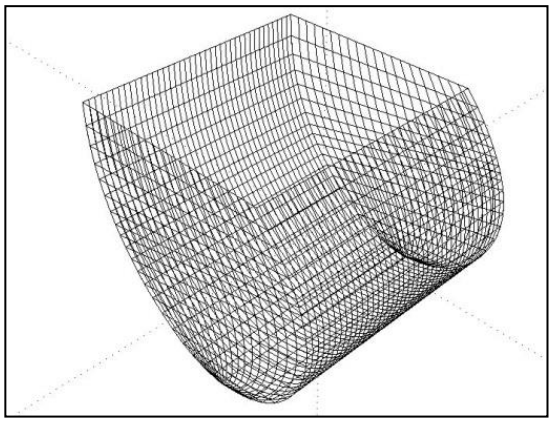

Fig. 5 Rotor with lower order panels using Multi-Surf

4.1 Validation

Procedure validation has been carried out by considering the Weptos rotor model (Rapuc 2012). The rotor tip has been placed in 'negative' x and the approach wave angle has been set at 0° which allows the waves to hit the tip of the rotor. Multi-Surf is used to discretize the rotor, a total of 1200 panels for the range of wave frequencies from 0.2 to 30 rad/s (see Fig. 5) and only half of the model have been considered for analysis due to symmetry in xz-plane. The model details are given in Table 2. The initial undisturbed free surface is considered at still water level (SWL) at z=0. The hydrodynamic coefficients added mass, damping and excitation forces has been obtained from WAMIT and compared with the Weptos rotor (Rapuc 2012). The present results from the WAMIT have been found to be good when compared with the Weptos rotor as shown in Figs. from 6(a)-6(c).

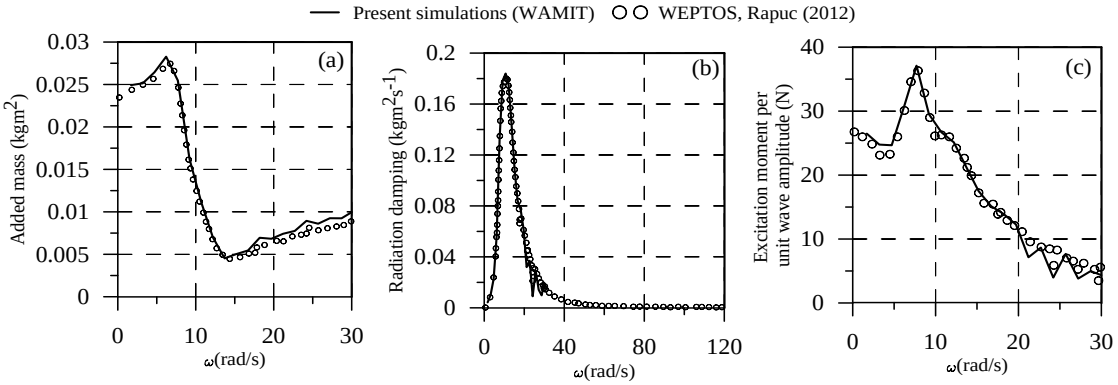

Fig. 6 Comparison of hydrodynamic coefficients (a) added mass (b) radiation damping and (c) excitation moment

Table 2 Weptos rotor model details

S. No	Weptos rotor	Value
1	Mass (kg)	4.29
2	Center of gravity (from SWL) (m)	-0.0277
3	Mass moment of inertia (kg.m^2)	4.94E-02
4	Width (m)	0.24
5	Depth of submergence (m) from SWL	0.107
6	Water depth (m)	0.81

4.2 Viscous damping

The effect of damping due to the various geometric parameters on pitch response of the WEC rotor is investigated by conducting free decay test using STAR-CCM+. All the computations have been performed on an Intel® Core™ i7-7700 CPU @ 3.6 GHz computer with 16 GB RAM. The dependency of the domain and mesh are carried out before arriving at the final sizes of the flow problem. The computational domain is set in right handed coordinate system *Oxyz* with the origin at center of the WEC, *z*-axis positive upwards and the free surface level has been changed based on the depth of submergence and *x*-direction is for propagation of generated waves from the WEC (see Fig. 7). The flow is controlled by the boundary conditions assigned to the different regions in the domain. The initial pressure and velocity are set to the hydrostatic pressure and inlet velocity. The problem is analyzed as two dimensional (2D); the *y*-direction is essentially ignored. A quasi 2D simulation with the less number of elements in *y*-direction is implemented. The flow problem is solved by using the three dimensional continuity, momentum and turbulent k-epsilon model without modifying the default settings. Volume of fluid (VOF) is used to track the free surface in the various fluid phases and where in all the phases share velocity and pressure fields. The pitch response has been obtained by an overset mesh technique or also called as overlapping meshes. Two separate regions are created, one corresponds to background region and another surrounding the WEC (acts like an overset), required information is allowed between two regions through the overlapping cells. In the present study, linear data interpolation is used to couple the solution in the overset and background regions (see Hadzic 2006). To reduce the wave reflections from the both ends of the computational domain VOF damping is enabled. The analysis is carried out with a second order implicit unsteady time integration with five inner iterations for convergence of the residual values. Dynamic fluid body interaction (DFBI) with fixed center of translation/rotation about the origin in single degree of freedom is used.

The computational domain is -200 m to +200 m in *x*-direction, -2.5 m to +2.5 m in *y*-direction and -10.0 m to +8.0 m in *z*-direction. The domain has been defined into several parts with different mesh sizes. Fine dense mesh is used where the flow variables have large gradients, i.e., at the free surface and at the WEC regions (see Fig. 7).

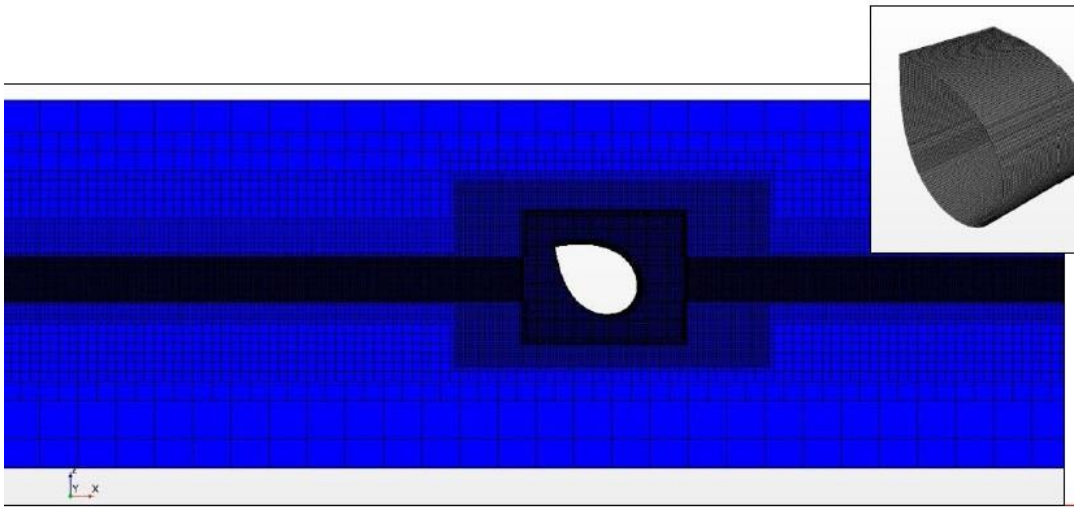

Fig. 7 Initial mesh generation around the computational domain. (Insert photo shows the mesh on the WEC rotor)

The domain is discretized into small cells with trimmed cell mesher, base size of 5 m in background region and 2.0% of the background base size in overset region is defined to produce a high-quality grid predominantly by hexahedral elements in the computational domain; surface remesher is selected to generate mesh around the WEC rotor and prism layer for treating the boundary layer. A prism layer of thickness 0.1 m with 10 number. of elements is selected. The total number of cells is about 0.46million in background region and 0.16 million in the overset region. Fig. 7 shows the discretized domain in and around the WEC. The damping zone length of 100m is enabled on both sides of the computational domain.

The decay test is conducted with an initial pitch angle negative 30° given from the rest position and the rotor is allowed to move freely in the calm water (see Fig. 8(a)). Fig. 8(b) shows a typical decaying time-history data for a WEC rotor D0.7a60. For large angles of rotation, rotor may experience the nonlinear effects and these are subjected to change case by case, so a typical WEC rotor is chosen for quantification. Free decay test has been carried out on a WEC rotor D0.7a60 by keeping the kinematic viscosity zero. A difference of about 40% is noted when compared to the WAMIT radiation damping. This difference can be attributed to the nonlinear effects. To ascertain, this needs further nonlinear time domain wave-structure interaction which are kept out of the present scope. The classic way to extract the damping coefficient from free decay test is the logarithmic-decrement method. The damping ratio can be obtained from the successive peaks in the free decay data is given by

$$\chi = \frac{1}{\sqrt{1+\left(\frac{2\pi}{\ln\left(Z_{w1}/Z_{w3}\right)}\right)^2}} \; or \; \chi = \frac{1}{2\pi}\ln\left(\frac{Z_{w1}-Z_{w2}}{Z_{w3}-Z_{w4}}\right) \tag{13}$$

where Z_{w1}, Z_{w2}, Z_{w3} *and* Z_{w4} are the successive peaks of the pitch free decay response.

The critical damping (C_{cr}) can be obtained as $2(J+A_{55})\,\omega_N$. The damping ratio is by definition the ratio between the actual damping(C_a) and critical damping. The viscous damping can be estimated by subtracting the radiation damping from the actual damping. Viscous damping values from the STAR-CCM+, radiation damping values from the WAMIT analysis for the various WEC rotors are listed in Table 3. The obtained viscous damping will be included as an external damping in the equation of motion (Eq. 4(b)).

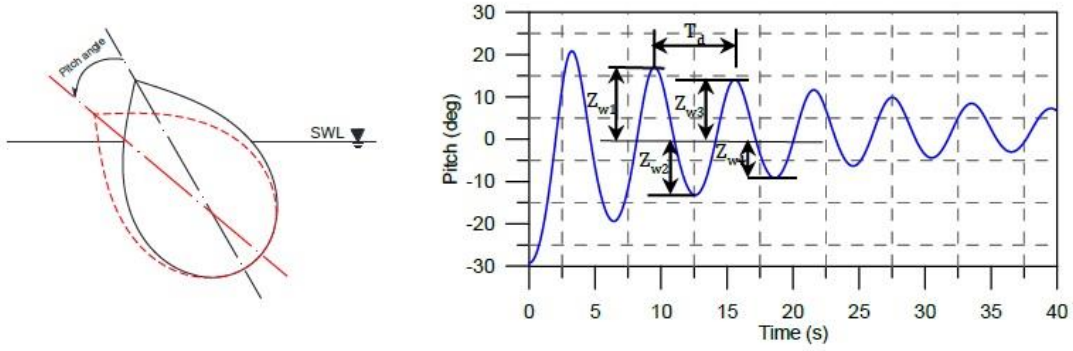

Fig. 8 Pitch free decay test (a) Initial angle to WEC rotor and (b) Typical free decay data of the WEC rotor (D0.7a60) where zero corresponds to initial beak angle (60deg)

5. Results and discussion

The hydrodynamic coefficients have been evaluated for various panel sizes to obtain the converged panel size over range of frequencies between 0.1 to 6.0 rad/s in a water depth of 80m. Finally, the No. of panels of 1300 has been chosen for the rest of analysis see Fig. 9.

Table 3 Damping ratio, radiation damping and viscous damping for various WEC rotors

Cases	Natural frequency (rad/s)	Damping ratio (χ)	Radiation damping (ton.m.s^{-1})	Critical damping (ton.m.s^{-1})	Viscous damping (ton.m.s^{-1})
D0.7a36	1.53	0.123	27.38	433.97	25.79 (49)
D0.7a48	1.56	0.129	28.64	431.42	27.08 (49)
D0.7a60	1.03	0.036	2.61	218.84	5.35 (67)
D0.8a36	1.57	0.170	42.96	574.21	54.60 (56)
D0.8a48	1.335	0.137	15.93	387.04	37.08 (70)
D1.05a60	1.05	0.113	9.60	474.65	44.13 (82)

Note: Values in the last column in parenthesis indicates the percentage of the viscous damping with respective to the actual damping

The center of rotation of WEC rotor placed at the body-fixed coordinate in WAMIT which allow pitching around the right axis. A WEC rotor (see Fig. 3) is having a cylindrical hole centered on the axis of rotation '*O'* but from the Fig. 9 one can notice that the rotor without hole is considered for WAMIT analysis. It is needless to consider the WEC rotor with hole in the analysis due to the fact that added mass, damping, exciting force and hydrostatic moment will not change if the hole is fully submerged. So, the mesh used for WAMIT calculation has therefore been made without considering the hole (see Fig. 9). The WEC rotor has been trimmed to the required draft in calculation. Wave amplitude of 1.0 m is considered for the study. The required hydrodynamic coefficients added mass, damping and excitation moment were obtained and shown in Figs. 10-12.

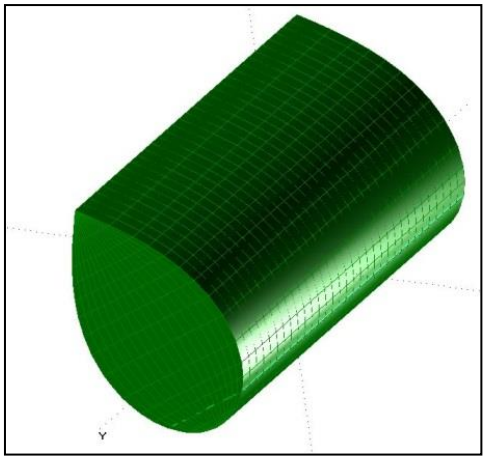

Fig. 9 Mesh generation using Multi-surf

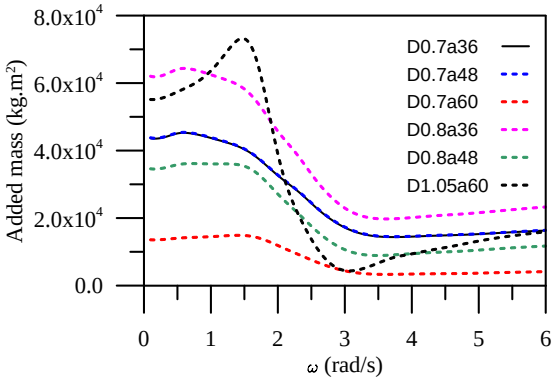

Fig. 10 Pitch added mass

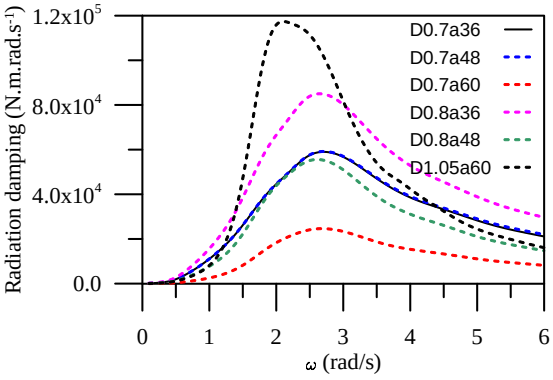

Fig. 11 Pitch radiation damping

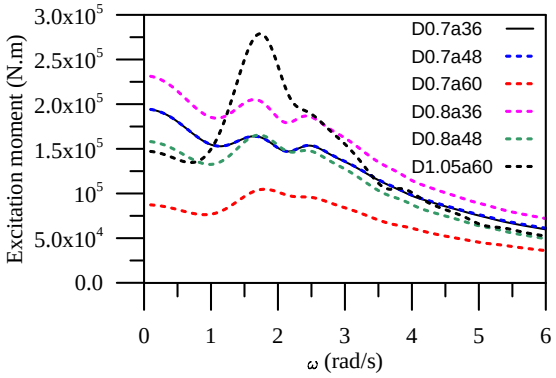

Fig. 12 Pitch excitation moment

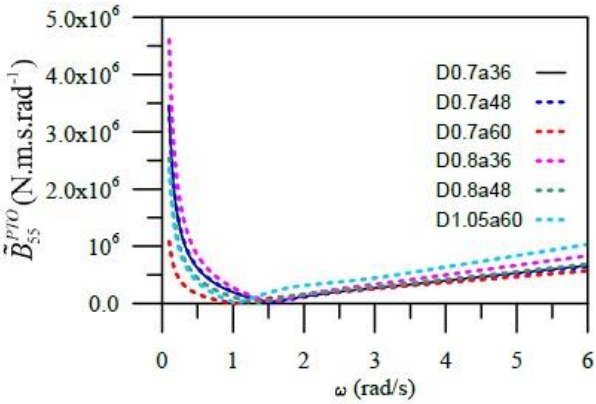

Fig. 13 PTO damping

Fig. 10 shows the added mass as a function of wave frequency for various WEC rotors. The added mass increases with the increase in the depth of submergence and decreases with increase in the beak angle. Similar trend is followed for the radiation damping and excitation force sees Figs. 11~12. This is expected since all hydrodynamic coefficients depend on the wetted surface of the WEC rotor geometry. PTO damping estimated by Eq. (6) for various WEC rotors is shown in Fig. 13. From Eq. (8) it is evident that the response is one of the key parameter which defines the performance of the WEC rotor. The final pitch response is obtained by solving the linear equation of motion of WEC rotor using Eq. 4(b) with the available hydrodynamic coefficients obtained from WAMIT, viscous damping from the STAR-CCM+ and estimated PTO damping by Eq. (6) (see Fig. 13). Figs. 14 and 15 show the variation of the pitch response of the WEC rotor without and with viscous damping for the range of wave frequencies. For a constant depth of submergence, the increase in the beak angle increases the pitch response of the WEC rotor whereas it is in-consistence for the vice-versa (see Figs. 14 and 15).

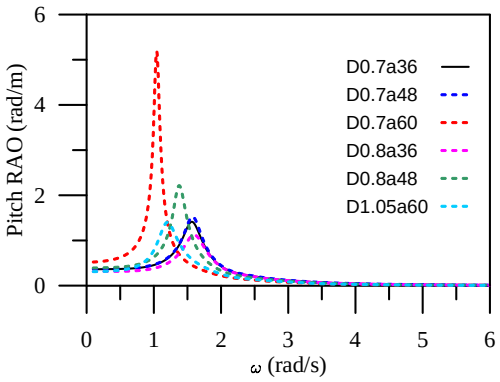

Fig. 14 Pitch response without viscous damping

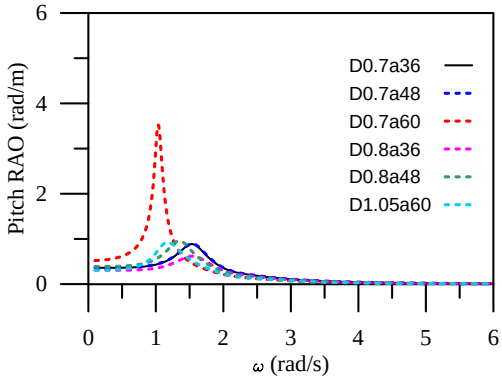

Fig. 15 Pitch response with viscous damping

Table 3 gives the obtained viscous damping for the WEC rotor from the free decay test. 82% of total damping and 0.9-4.6 times when compared to the radiation damping. It is evident that the effect of viscous damping is predominant in most of the rotors. The higher the beak angle and depth of submergence, the higher the value of viscous damping. With the addition of viscous damping, the pitch response is notably reduced by highest 57% for D0.8a48 and lowest 32% for D0.7a36 (Table 4) when compared to without viscous damping. Finally, comparison of the mean optimal power and capture width for without and with viscous damping for the various WEC rotors has been given in Figs. 16 to 19. The mean optimal power and capture width are overestimated without inclusion of the viscous damping see Figs. 16 and 18. It is shown that the incorporation of viscous damping causes quite significant loss in the mean optimal power and capture width see Fig. 17 and 19. The WEC rotor D0.7a60 with viscous damping, which is 2.8 m draft at 60° beak angle, gives the maximum optimum power of 81.8kW/m^2 when compared with the other rotors in regular waves.

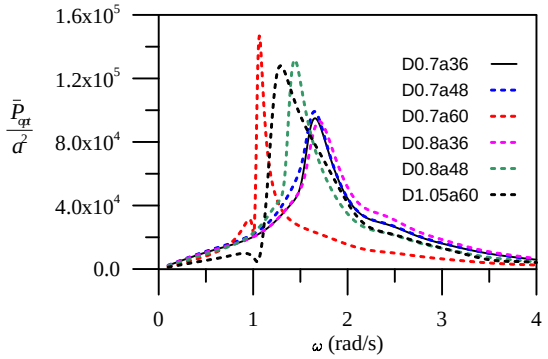

Fig. 16 Maximum mean power without viscous damping

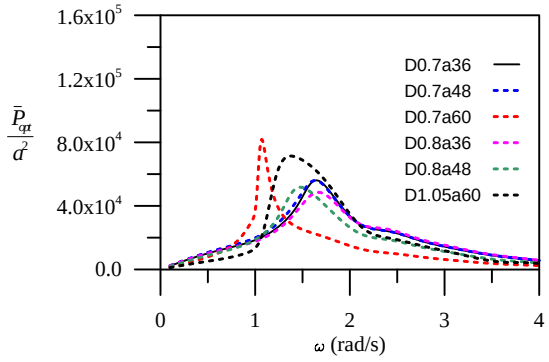

Fig. 17 Maximum mean power with viscous damping

Table 4 Maximum pitch response and maximum mean optimal power for various WEC rotors

Cases	Maximum pitch response (rad/m)		Maximum pitch response percentage reduction	Maximum mean optimal power, $\frac{\bar{P}_{opt}}{a^2}$ (kW/m^2)		Percentage reduction of $\frac{\bar{P}_{opt}}{a^2}$
	Without viscous	With viscous		Without viscous	With viscous	
D0.7a36	1.41	0.89	37	94.9	56.1	41
D0.7a48	1.53	0.89	42	99.2	56.0	43
D0.7a60	5.18	3.53	32	146.8	81.8	44
D0.8a36	1.13	0.62	45	93.0	48.5	48
D0.8a48	2.21	0.96	57	131.8	51.8	61
D1.05a60	1.40	0.93	34	128.0	71.4	44

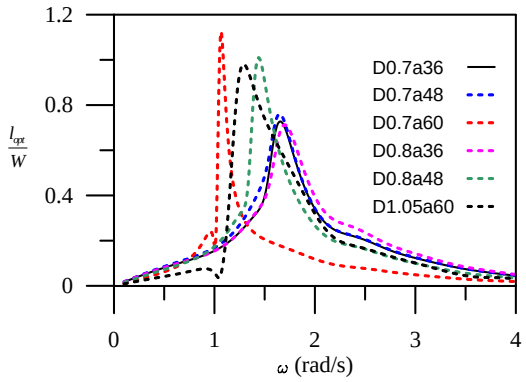

Fig. 18 Optimum capture width without viscous damping

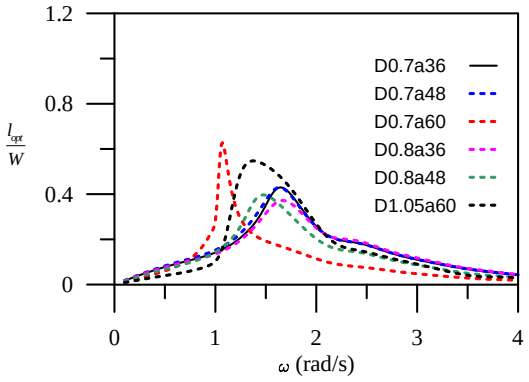

Fig. 19 Optimum capture width with viscous damping

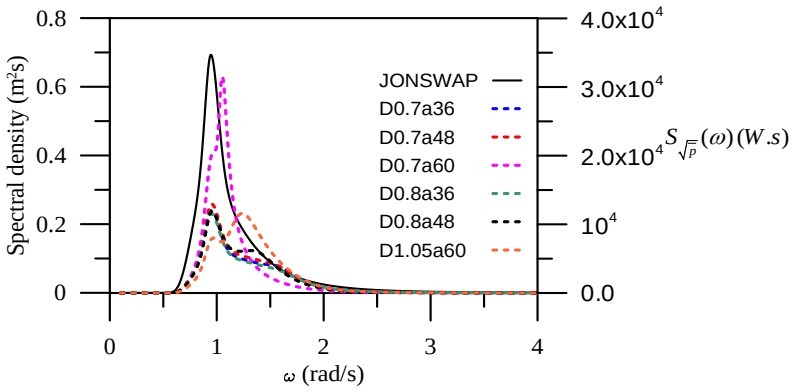

Fig. 20 JONSWAP spectrum of the installation site along with the square-root of power spectral response with viscous damping ($S_{\sqrt{\bar{P}}}$)

Now, estimation of the WEC rotor response in irregular waves will be considered. As explained in the section 3, the sea conditions at the Jeju western coast at the Chagwido site represented by JONSWAP wave spectrum can be seen in black solid line in Fig. 20. The wave spectrum with peakedness factor $\gamma = 2.2$, significant wave height ($H_{1/3}$) of 2.0 m and peak period (T_p) of 6.65s is used. The square-root of power spectral response (see Eq. (12)) is obtained from the mean optimal power by the sea spectrum with a linear assumption as shown in dotted lines in Fig. 20.

Two peaks can be seen in the square-root of power spectral response where one peak corresponds to the peak wave frequency 0.944 rad/s and an additional peak near the natural frequency of WEC rotors. With the variation in the peak frequencies a significate reduction in the power can be noticed from Fig. 20. In comparison among the other WEC rotors, the square-root of average extracted power ($\bar{P}_{irr}$) is 9.2kW for D0.7a60 rotor with viscous damping and whose natural frequency is 1.03 rad/s, closest to the wave frequency of the installation site.

6. Conclusions

The hydrodynamic performance of the WEC rotor has been studied based on linear potential flow theory using both WAMIT and CFD for various rotors for different beak angles and depth of submergence. The hydrodynamic coefficients increase with the increase in the depth of submergence and decrease with the increase of beak angle. For a constant depth of submergence, the increase in the beak angle increases the pitch response of the WEC rotor whereas it is in-consistence for the vice-versa. The effect of viscous damping on the pitch response of the WEC rotor is investigated by conducting free decay test using STAR-CCM+. Logarithmic-decrement method is used to obtain the viscous damping from the free decay data. In the present study the WEC responds only in single degree of freedom and in this case considerable damping through the PTO can be seen but it is significant due to the viscous damping. The sensitivity of WEC rotors extractable power evaluation to the local Jeju western coast has been carried out using JONSWAP

spectrum. The performance of WEC rotor with depth of submergence 2.8m and beak angle 60° was shown to be efficient in both regular and spectral waves. It would be interesting to extend further investigation in time domain analysis where the nonlinear interaction effects can be properly taken into consideration which is under progress.

Acknowledgments

This research was supported by the 2017 scientific promotion program funded by Jeju National University.

References

Antonio, F.D.O. (2010), "Wave energy utilization: A review of the technologies", *Renewable and sustainable energy reviews*, **14**(3), 899-918.

Bhattacharyya, R. and McCormick, M.E. (2003), *Wave Energy Conversion*. Elsevier ocean engineering book series, Oxford, UK.

Chakrabarti, S. (2005), *Handbook of Offshore Engineering*, Elsevier, Amsterdam, Netherlands.

Cho, I.H. and Kim, M.H. (2013), "Enhancement of wave-energy-conversion efficiency of a single power buoy with inner dynamic system by intentional mismatching strategy", *Ocean Syst. Eng.*, **3**(3), 203-217.

Cho, I.H., Kim, M.H and Kweon, H.M. (2012), "Wave energy converter by using relative heave motion between buoy and inner dynamic system", *Ocean Syst. Eng.*, **2**(4), 297-314.

Count, B.M. (1978), "On the dynamics of wave-power devices", *P. Roy. Soc. London A: Math., Phys. Eng. Sci.*, **363**(1715), 559-579.

Cruz, J. (2007), *Ocean Wave Energy: Current Status and Future Perspectives*. Springer Science & Business Media, Berlin, Germany.

Evans, D.V. (1976), "A theory for wave-power absorption by oscillating bodies", *J. Fluid Mech.*, **77**(1), 1-25.

Falnes, J. (2002), *Ocean Waves and Oscillating Systems: Linear Interactions including Wave-Energy Extraction*, Cambridge University Press, Cambridge, UK.

Falnes, J. (2007), "A review of wave-energy extraction", *Mar. Struct.*, **20**(4), 185-201.

Folley, M. (Ed.) (2016), *Numerical Modelling of Wave Energy Converters: State-of-the-Art Techniques for Single Devices and Arrays*, Academic Press, Cambridge, MA, USA.

Hadzic, H. (2006), "Development and application of finite volume method for the computation of flows around moving bodies on unstructured, overlapping grids", Ph.D. Dissertation, Technical University Hamburg-Harburg, Hamburg, Germany.

Jeffrey, D.C., Richmond, D.J.E. and Salter, S. (1976), *Second year interim report on Edinburgh Wave Power Project: Study of mechanisms for extracting power from sea waves*, University of Edinburgh, Edinburgh, UK.

Kim, J.R., Bae, Y.H. and Cho, I.H. (2014), "Design of wave energy extractor with a linear electric generator-part I. design of a wave power buoy", *J. Korean Soc. Mar. Environ. Energy*, **17**(2), 146-152.

Mei, C.C. (1976), "Power extraction from water waves", *J. Ship Res.*, **20**, 63-66.

Mei, C.C., Stiassnie, M. and Yue, D.K.P. (2005), *Theory and Applications of Ocean Surface Waves: Nonlinear Aspects*, World scientific, Singapore.

Mynett, A.E., Serman, D.D. and Mei, C.C. (1979), "Characteristics of Salter's cam for extracting energy from ocean waves", *Appl. Ocean Res.*, **1**(1), 13-20.

Pecher, A., Kofoed, J.P. and Larsen, T. (2015), "The extensive R&D behind the Weptos WEC", *Renew. Energ. Offshore*, 351-358.

Pecher, A., Kofoed, J.P., Larsen, T. and Marchalot, T. (2012), "Experimental study of the Weptos wave energy converter", *Proceedings of the 31st International Conference on Ocean, Offshore and Arctic Engineering*, Rio de Janeiro, Brazil, July.

Pizer, D. (1994), *Numerical Modelling of Wave Energy Absorbers*. Harwell Laboratory, Energy Technology Support Unit, UK.

Rapuc, S. (2012), "Numerical study of the WEPTOS Single Rotor", Doctoral dissertation, Master Thesis report, Aalborg University and Technical University of Denmark, Denmark.

Salter, S., Jeffrey, D.C. and Taylor, J.R.M. (1975), *First year interim report on Edinburgh Wave Power Project: Study of mechanisms for extracting power from sea waves*, University of Edinburgh, Edinburgh, UK.

Salter, S.H. (1974), "Wave power", *Nature*, **249**(5459), 720-724.

Skyner, D. (1987), *Solo Duck Linear Analysis*, University of Edinburgh, Edinburgh, UK.

MK